Science Advances
AAAS

advances.sciencemag.org/cgi/content/full/5/6/eaax3800/DC1

Supplementary Materials for

Breaking the quantum adiabatic speed limit by jumping along geodesics

Kebiao Xu, Tianyu Xie, Fazhan Shi, Zhen-Yu Wang*, Xiangkun Xu, Pengfei Wang, Ya Wang, Martin B. Plenio, Jiangfeng Du*

*Corresponding author. Email: zhenyu.wang@uni-ulm.de (Z.-Y.W.); djf@ustc.edu.cn (J.D.)

Published 21 June 2019, *Sci. Adv.* **5**, eaax3800 (2019)
DOI: 10.1126/sciadv.aax3800

This PDF file includes:

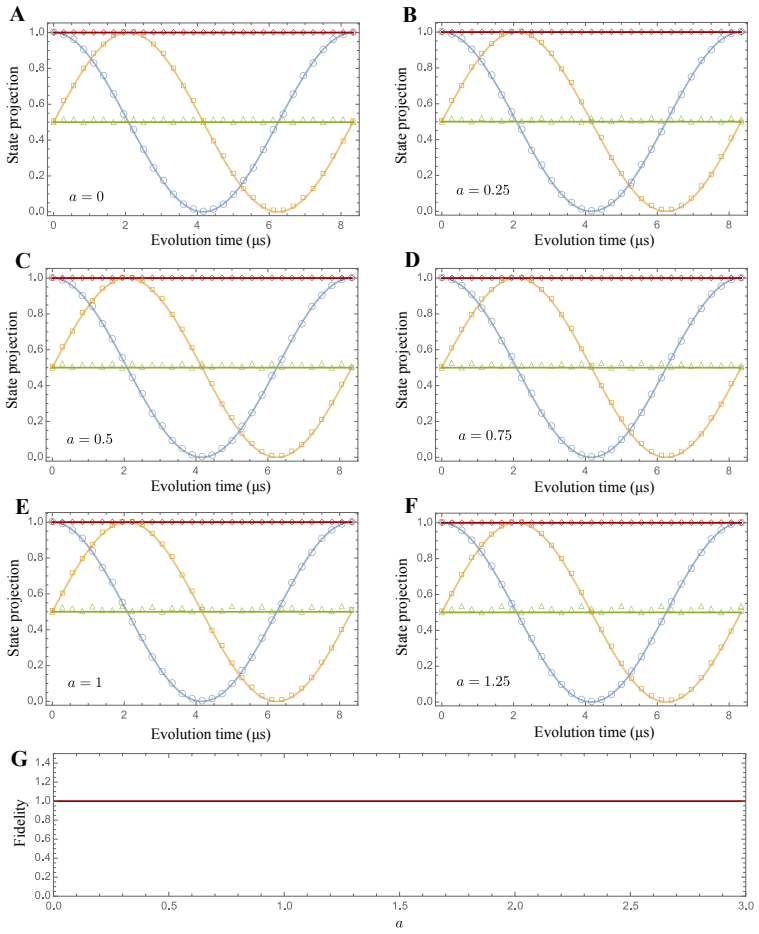

Fig. S1. Transition of adiabatic control from a constant gap to a gap with energy level crossings. (**A** to **F**) Simulated projections of the state driven by the adiabatic protocol as in Fig. 1 in the main text but using different values of a in the energy gap $\Omega_\pi(\lambda) = \Omega_0' \left[1 + a\cos(2\Omega_0' T\lambda)\right]$. Diamonds show the projection to the ideal adiabatic state $|+_\lambda\rangle$ (i.e., fidelity of adiabatic evolution) during the evolution time $t = T\lambda$. The state projections to $|\mathrm{x}\rangle$ (circles), $|\mathrm{y}\rangle$ (squares), and $|\mathrm{z}\rangle$ (triangles) are also shown to demonstrate the evolution of the adiabatic process. Solid lines are the case of a perfect adiabatic evolution (e.g., for $T \to \infty$). For $a = 0$, the control is the conventional adiabatic driving with a constant gap (see Fig. 1D in the main text for experimental results). Increasing the parameter to $a = 1$ will close the gap at $t = \pi/(2\Omega_0')$. When $a > 1$, there are energy level crossings (see Fig. 1H in the main text for experimental results). (**G**) Calculated adiabatic fidelity of the final state at time $t = T$ as a function of a. The amplitudes $\Omega_0' = \sqrt{2/(2+a^2)}\Omega_0$ are used to have the same average microwave power in all plots and hence is smaller than $\Omega_0 = 2\pi \times 6$ MHz. All plots demonstrate that the state follows the adiabatic evolution with high fidelity.

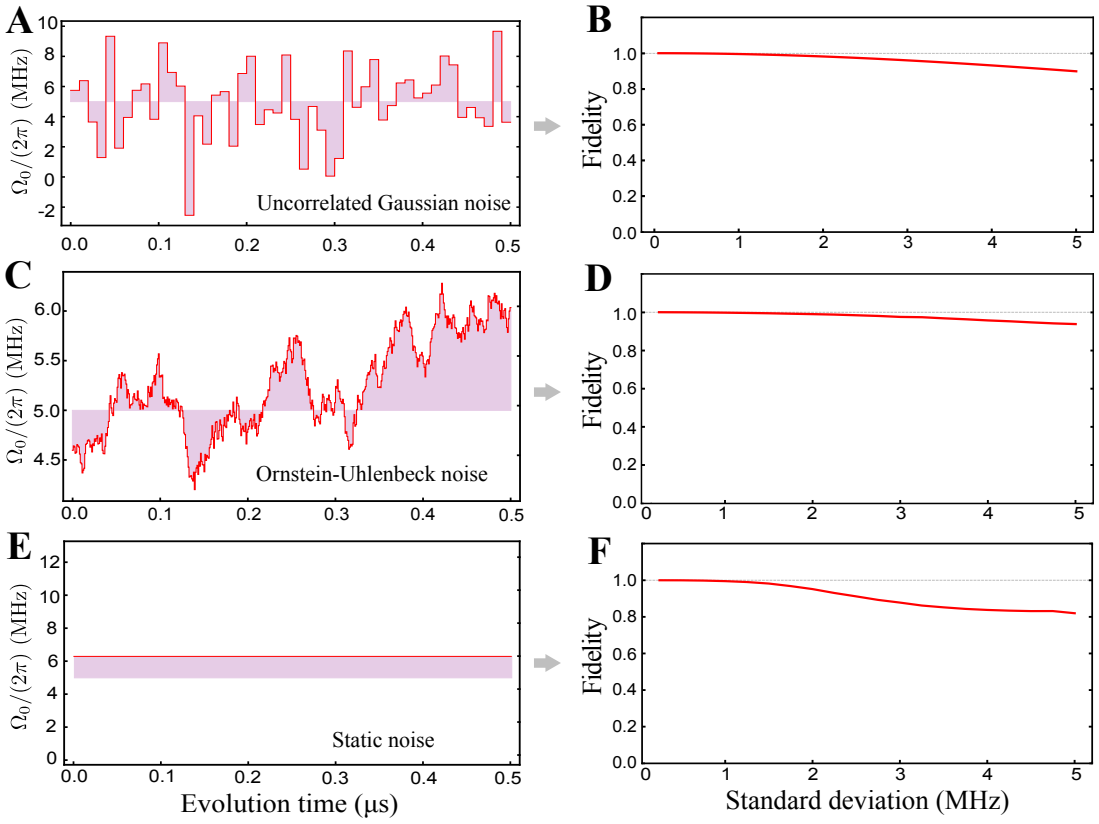

Fig. S2. Robustness of the jumping protocol against different kinds of control noise. (**A**, **C**, and **E**) Exemplary time traces of the driving Rabi frequency for a mean of $2\pi \times 5$ MHz and a standard deviation of $2\pi \times 2.5$ MHz. (**B**, **D**, and **F**) Simulated fidelity of adiabatic evolution for the jumping protocol with a total time $T = 0.5$ μs and a Rabi frequency of $2\pi \times 5$ MHz as a function of the standard deviation of the applied noise illustrated in (A), (C), and (E). The simulations have been averaged over 10^4 random time traces of noise. While the fidelity decays as the strength of the noise in the Rabi frequency increases, the fidelity of the jumping protocol remains high for a wide range of noise amplitudes. Three types of noise on the Rabi frequency of the control pulses are studied in the simulation: the white noise with the uncorrelated Gaussian distribution on the amplitudes in (A) and (B), the Ornstein-Uhlenbeck process modeled noise in (C) and (D), and the static noise in (E) and (F). The amplitudes of the Gaussian distributed noise in (A) are uncorrelated at every slices of duration of 10 ns. The Ornstein-Uhlenbeck process modeled noise in (C) satisfies the following differential equation: $dX_t = -\beta(X_t - \alpha)dt + \sigma dW_t$, where $\alpha = 2\pi \times 5$ MHz is the mean value and σ is the standard deviation; W_t is modeled by the Wiener process $f_{W_t(x)} = \frac{1}{\sqrt{2\pi t/t_0}} e^{-x^2/(2t/t_0)}$ with $t_0 = 1$ μs; the decay rate $\beta = 10$ s^{-1} and the time slice $dt = 1$ ns are used in the simulation. The static noise in (E) has a random constant amplitude over each run of the adiabatic protocol with a Gaussian distribution.

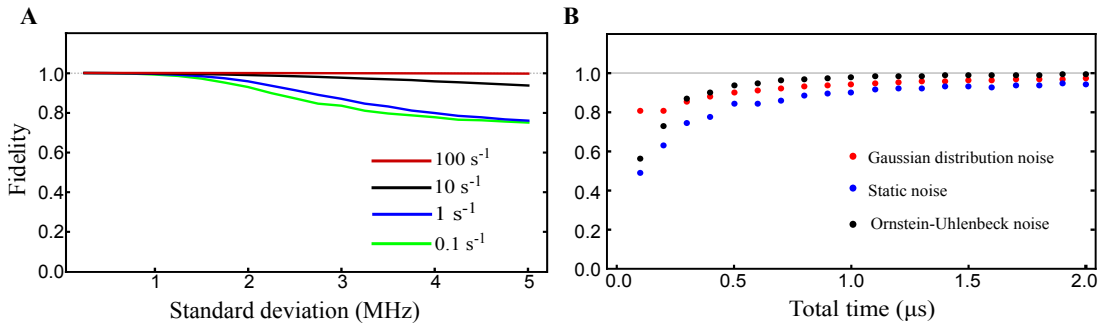

Fig. S3. Enhancing the robustness of jumping protocol in the presence of control noise. (**A**) Simulated fidelity to the ideal adiabatic state at the final time of evolution for different decay rates β in the Ornstein-Uhlenbeck process modeled noise. The red, black, blue, and green lines correspond to $\beta = 100$, 10, 1 and 0.1 s^{-1}, respectively. The simulations in (A) show that the fidelity of the jumping protocol decays slower with the increase of the noise strength when the decay rate β goes higher. (**B**) Simulated fidelity to the ideal adiabatic state at the final time of evolution for different kinds of noise. The jumping protocol uses a driving Rabi frequency with a mean of $2\pi \times 5$ MHz. The results in (B) show that in the presence of control errors the fidelity of the jumping protocol can be increased by increasing the total time T for adiabatic evolution. The red, blue, and black dots correspond to the uncorrelated Gaussian distribution noise, static noise, and Ornstein-Uhlenbeck process modeled noise, respectively. The parameters in these noise models are the same as the ones chosen in fig. S2.

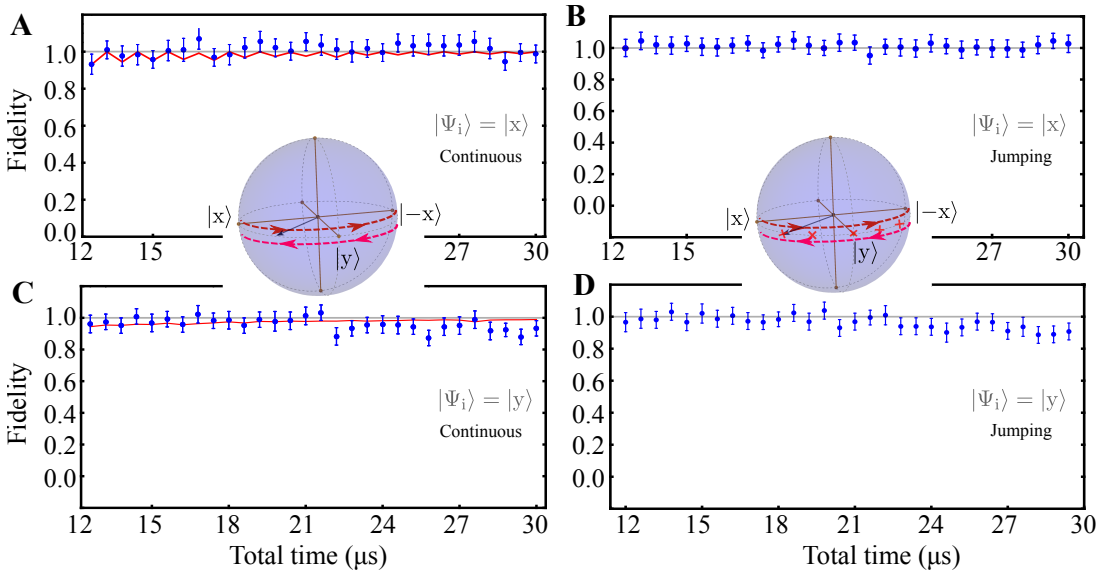

Fig. S4. Coherence protection during adiabatic evolutions. (**A** to **D**) Fidelity to the ideal adiabatic state at the final evolution as a function of the total time that is much larger than the NV coherence time $T_2^* = 1.7$ μs without control. The evolution path, the control parameters, as well as the meaning of the blue dots (experiment) and red lines (simulation) are the same as those used in Fig. 4 in the main text. (A) and (C) Results for the continuous protocol with a constant gap. (B) and (D) Results for the jumping protocol. In (A) and (B) the initial state was prepared in $|x\rangle$, while in (C) and (D) the initial state was prepared in $|y\rangle$.

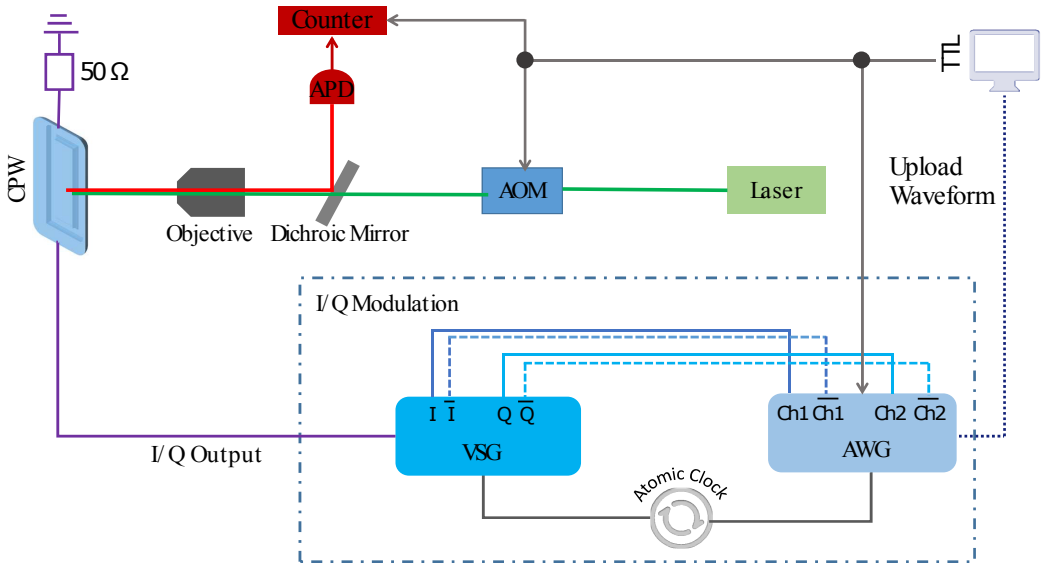

Fig. S5. Sketch of the experimental setup. The whole setup mainly consists of two parts: a home-built confocal microscopy and a microwave synthesizer. The microwave used to control the spin evolution was generated through I/Q modulation. The desired waveform was uploaded form the PC to the AWG. The two separated channels on the AWG generated the I and Q signal respectively and transmitted to the VSG, then the VSG did the I/Q modulation. An atomic clock was used to synchronize the AWG and VSG. A pulse blaster served to provide TTL signals to control the switch of the AWG and AOM, and also the time bin of the counter.

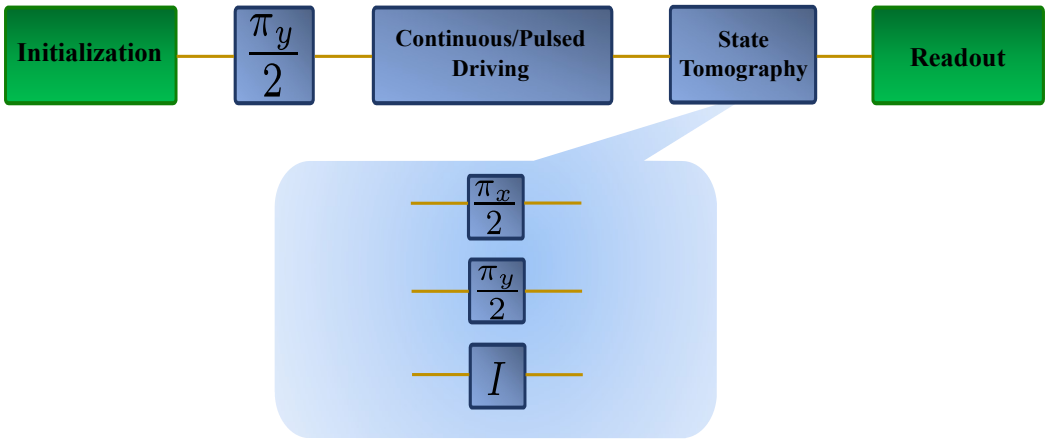

Fig. S6. Experimental pulse sequence. Green laser was applied in the beginning to initialize the electronic spin and at the end to readout the spin state. The first $\pi_y/2$ pulse is used to set the spin state to be aligned with $+x$ axis. The continuous or pulsed protocol drives the spin state for quantum adiabatic evolution. When doing the quantum state tomography, three different kinds of pulses were applied, i.e., $\pi_x/2$, $\pi_y/2$, or the identity operator.